To be published in Nuclear Instruments and Methods (A) SRF030520-15

Suppression of Multipacting in Rectangular Coupler Waveguides

R.L. Geng *, H. Padamsee, S. Belomestnykh

Laboratory for Elementary Particle Physics, Cornell University, Ithaca, NY14853, USA

P. Goudket, D.M. Dykes

ASTeC, CLRC Daresbury Laboratory, Warrington WA4 4AD, UK

R.G. Carter

Engineering Department, Lancaster University, Lancaster LA1 4YR, UK

Abstract

Although a rectangular waveguide coupler has the conceptual advantages of simplicity and capability of withstanding higher power, builders of modern superconducting accelerators are routinely choosing instead a coaxial coupler for its proven performance. Multipacting induced discharge has been found to be an operating mechanism that prevents a rectangular waveguide coupler from reaching its full potential. Earlier calculations predicted the existence of two-sided multipacting in a rectangular waveguide geometry. In the present study, special waveguide sections of CESR type were built and tested. Multipacting characteristics of the waveguide were identified. Two multipacting suppression methods, the slotted waveguide method and the DC magnetic bias method, were experimentally evaluated. The multipacting current is suppressed by a factor of more than 2 by opening a slot on the broad wall. Complete multipacting suppression can be realized by using the DC magnetic bias method.

Key words: Multipacting, Coupler waveguide, DC magnetic bias, Slotted waveguide
PACS: 52.80.Vp, 52.80.Pi, 84.40.Az

* Corresponding author.
Email address: rg58@cornell.edu (R.L. Geng).

1 Introduction

Rectangular waveguide couplers are widely used in superconducting, as well as normal conducting, RF systems for feeding power into RF resonators. Examples of such applications include accelerators such as CEBAF, CESR and PEP-II, and light sources such as SRRC, CLS, and DIAMOND. With the increasing demands for beam power and system stability, the performance of RF couplers becomes critical to the smooth operation of these machines. The most notable coupler problems are related to ceramic RF windows, which serve as the air-vacuum barrier for RF cavities. These problems include thermal induced ceramic failure and multipacting on the ceramic surface of the vacuum side. In recent years, increasing attention has been paid to the coupler waveguide section between the ceramic window and the coupler-cavity interface. This is particularly true for a superconducting RF system, because the coupler waveguide section in such a system is subject to cryogenic cooling, which has important impact on the design and operation of RF couplers.

With the application of high power couplers in modern high luminosity colliding machines, it has become increasingly clear that multipacting caused breakdown in the coupler waveguides can disturb or even limit the machine performance. This is true not only for rectangular waveguide geometry, but also for coaxial ones. Multipacting in coaxial type couplers has been well demonstrated both through experimental studies and numerical simulations [1][2][3][4]. The successful DC electric bias method was first introduced by Tückmantel et al [1] to suppress multipacting in LEPII coaxial couplers. The effectiveness of this method was soon borne out also by systematic numerical simulations [5]. The importance of having such an active multipacting suppression method is now being appreciated by designers of modern high power couplers. The reason is that a multipacting-free coupler design can be difficult, if not impossible, to realize due to constrains in practical situations. Without some method of multipacting suppression, the smooth operation of the coupler will have to rely on the so-called RF processing technique, which is often painstakingly time consuming. For this reason, the DC bias method has been widely adopted in coaxial couplers for various machines like KEK-B, LHC and SNS. It should be noted that the DC bias method was sometimes used differently. For example, it was used to promote, instead of suppress, multipacting during the period of coupler conditioning in KEK-B SRF systems [6]. In a recent study of coaxial couplers for SNS, the DC bias method was used for both purposes, namely promoting multipacting during conditioning period and suppressing multipacting after conditioning [7][8].

Exploration of multipacting in a rectangular waveguide coupler started in 1998, soon after the first CESR superconducting RF cryo-module was commissioned with a rectangular waveguide coupler designed for a power capability of

325kW. Multipacting showed up in the waveguide coupler when the RF power was first raised to the 90kW level. Frequent RF trips due to sharp vacuum bursts in the waveguide region were observed. To raise the power further, a special conditioning procedure, namely pulse processing, had to be applied repeatedly [9]. It then became desirable to study multipacting in the rectangular coupler waveguide of the CESR type. A 3D computer code, Xing, was developed to investigate multipacting characteristics in a rectangular waveguide geometry [10][11]. The simulation results revealed that two-point multipacting exists in the high electric field region. Two methods, one passive and the other active, have been proposed to suppress multipacting in a rectangular coupler waveguide. The passive method uses longitudinal slots in the broad walls. The active method, called the DC magnetic bias method (to mirror the DC electric bias method for a coaxial coupler), is to introduce a weak longitudinal DC magnetic field in the power transmission direction.

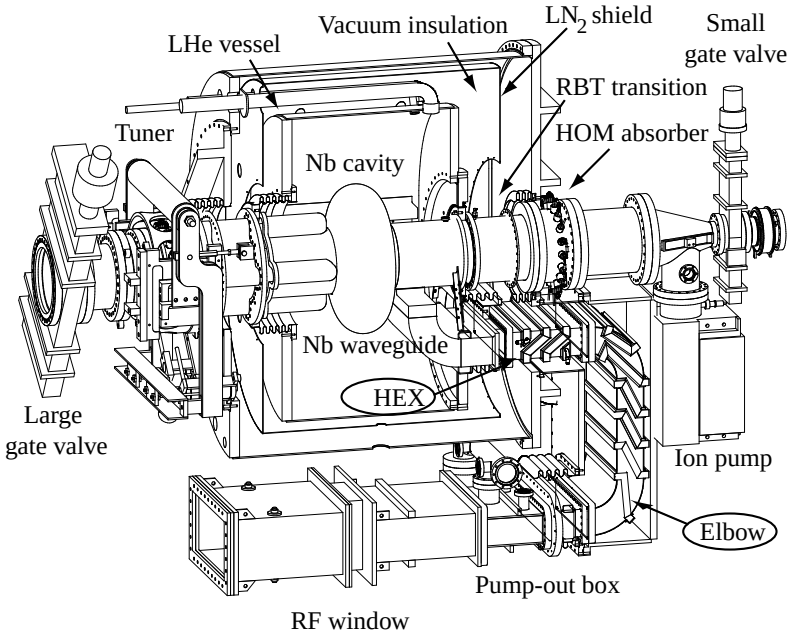

Fig. 1. Cryomodule of the CESR superconducting RF system. Solenoid coils are wrapped around the HEX and elbow sections of the waveguide coupler.

The DC magnetic bias method was briefly tested with an operating CESR cryo-module as shown in Fig. 1. Solenoid coils were wrapped around the heat exchanger (HEX) and the elbow sections of the waveguide coupler. Comparative observations were made before and after the elbow solenoid was activated. Before activation, sharp pressure bursts occurred in the coupler waveguide at particular forward power levels, which tripped off the RF. In contrast, after activating the elbow solenoid, which provided a longitudinal bias magnetic field of about 10 Gauss, the pressure in the coupler waveguide would instead oscillate for a while before developing into a final pressure burst, which again tripped off the RF. Unfortunately, the HEX coil was not explored at all during the test because of worries about the possible negative impact of its fringing

magnetic field on the Niobium cavity. The HEX waveguide section is expected to be more prone to multipacting due to its modified surfaces rich in cryo-sorbed species [12]. The result of this experiment was positive but not conclusive, because of the absence of a bias magnetic field in the HEX waveguide space. Nevertheless we were encouraged enough to keep the elbow coil activated during the later long-term CESR operations.

A comprehensive experimental exploration of the effectiveness of the bias magnetic method with an operating cryo-module was constrained by the boundaries imposed by the machine. The possible interference between the fringe magnetic field and the niobium cavity was a concern. The flexibility of changing the waveguide working mode was very limited. There was also a lack of necessary diagnostics, leaving the insights into the multipacting effect inaccessible. It became obvious that we needed to de-couple the coupler waveguide from the CESR machine and integrate important diagnostics into the test. For these reasons, we have designed and built two test waveguides of CESR type to experimentally verify the effectiveness of the proposed multipacting suppression methods. One waveguide is a regular CESR coupler waveguide, with which the multipacting characteristics are determined. It was also used to study the effectiveness of the bias magnetic method. The other waveguide has a groove on the bottom broad wall. Replaceable inserts can be fitted into the groove. This waveguide was used to study the effectiveness of the slotted waveguide method.

The primary objective of the present studies is to verify the multipacting suppression methods. Equally important, it is our desire to improve the understanding of fundamental aspects of multipacting in a coupler waveguide. In this paper, we will present the detailed results regarding the effect of the bias magnetic field and the slotted waveguide concept. Results regarding the fundamental aspects of waveguide multipacting, such as saturation effect, multipacting band discreteness and the direct cause of breakdown etc. will be published in a separate paper.

2 Experimental apparatus

The layout of the experimental set-up is depicted in Fig. 2

The multipacting waveguide section is fitted between two tapers transiting from the full-height (9 inches) to its half-height (4 inches) of a WR1800 waveguide. The upstream section leads to the 600 kW klystron (Philips YK1300), the downstream to the 300 kW water load. The test rig is situated between two E-plane bends so that observations can be made through view-ports at either end. Two Mylar windows (each 254 μm thick) are inserted between the

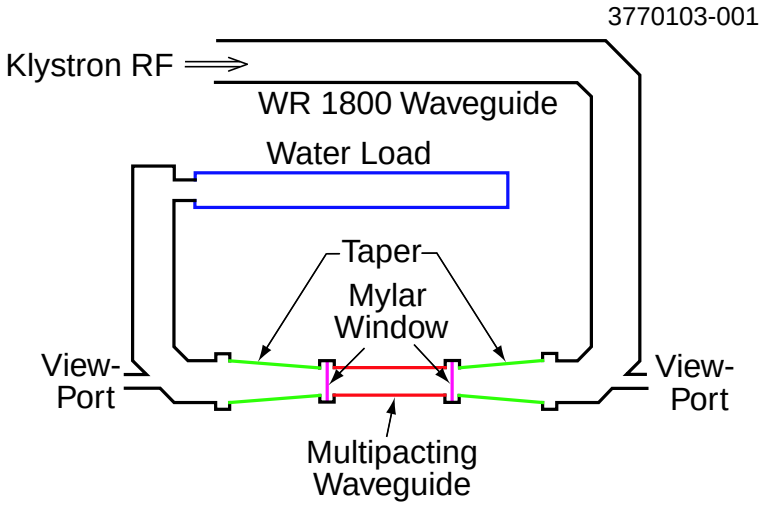

Fig. 2. Layout of the experimental set up.

test waveguide and the tapers so that a vacuum can be maintained in the test waveguide. The transparency of the Mylar films allows direct observation or image recording of the vacuum space where multipacting develops via the two view ports fitted on the bends.

Fig. 3 shows the 24-inch test waveguide along with the associated diagnostics. The cross section of the waveguide has a dimension of $18'' \times 4''$. The waveguide was fitted with a view port, an electron pickup probe (P1) and a photo-multiplier tube (PMT) on the side-wall. Three more electron pickup probes (P2, P3 and P4) and an electron energy analyzer (EEA) are distributed on the center-line of the top broad wall. The design of the EEA, which utilizes the retarding potential principle, closely follows that in [13]. Every electron probe was positively biased with a 24 V battery to facilitate the collection of the electrons and suppressing secondary electrons produced by the electron being collected. The opposite side-wall was fitted with two ports, one of which leads to a 50 L/s turbo pump and the other to a cold cathode gauge and an external pump out stand. A baseline vacuum in the mid-10^{-6} Torr range can be achieved within the test waveguide. The second waveguide is identical to the first except for a groove opened along the center line of the bottom broad wall. Inserts with different geometry or material can be fitted into the groove. Fig. 4 shows a cut-away view of the grooved waveguide and the insert fitted with a slotted copper bar.

Thermo-couples are attached to the outer surface of the waveguide for detecting multipacting induced temperature change and to the side-wall of the waveguide flanges for monitoring the temperature of the Mylar windows. Water-cooled copper bands are attached to the waveguide flanges to help cool the Mylar windows. An interlock system takes care of cutting off the RF in case the waveguide pressure is above 5×10^{-4} Torr or the PMT signal is over

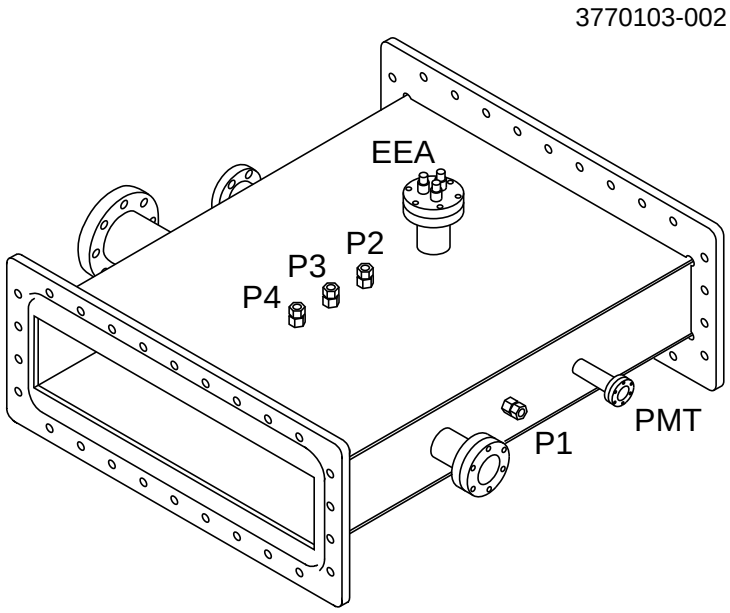

Fig. 3. Multipacting test waveguide with associated diagnostics including electron probes P1 through P4, the electron energy analyzer EEA and the PMT.

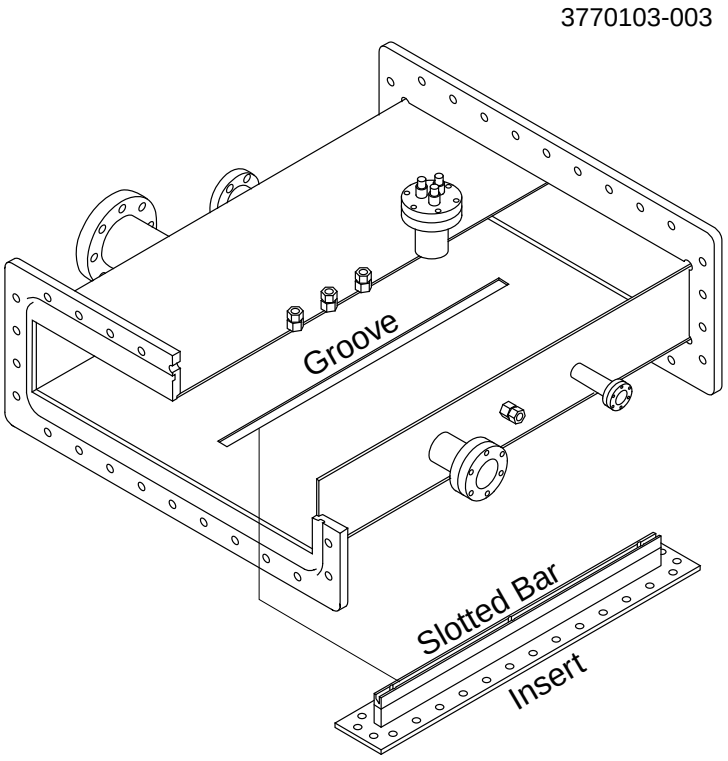

Fig. 4. Grooved waveguide. Inserts with different geometry or material can be fitted into the groove.

the preset threshold. The occurrence of an interlock interruption is most likely traced back to a multipacting-triggered breakdown. In several cases, the interlock was broken due to window rupture. The safety feature described above resembles that of the operating CESR cryo-modules, in which case an "RF trip" is recorded when a breakdown event occurs.

Experiments were conducted mainly in the traveling wave mode with a duty factor of 10% and the forward power being pulsed with a pulse length of about 2 ms. The RF pulse length has an important effect on the electrical activities in the waveguide space. If it is longer than 20 ms, multipacting will quickly induce gaseous breakdown. Since the objective of the present work is to study multipacting suppression, a short pulse length was chosen. Experiments were sometimes conducted in the standing wave or mixed wave modes. These were made possible by introducing a short plate or inductive iris at the junction between the downstream taper and the E bend.

3 DC magnetic bias

Earlier calculations with the code Xing predicted [10] that multipacting in the CESR coupler waveguide can be suppressed by applying a weak DC magnetic field along the wave propagation direction. This bias field bends the trajectories of multipacting electrons and hence perturbs the resonant condition that is needed for sustaining the multipacting. To verify the code predictions, the regular multipacting waveguide (see Fig. 3) was tested with and without the bias magnetic field. The bias magnetic field is provided by a solenoid coil wrapped around the entire multipacting waveguide, as illustrated in Fig. 5. Shown also in the figure are various diagnostic sensors, including electron pick-up probes, the electron energy analyzer and the PMT.

3.1 Multipacting characteristics of the waveguide

The multipacting waveguide was first tested comprehensively without the bias magnetic field. The existence of multipacting in the waveguide was clearly demonstrated by the detection of an electric current by the pick-up probes and the Faraday cup of the EEA. A stable multipacting current was obtained after the multipacting was allowed to burn (a process that has been commonly referred to as RF processing), for various durations depending on the history of the waveguide surface. Fig. 6 shows the multipacting current measured by the Faraday cup before and after the RF processing when the waveguide was operated in a traveling wave mode. It is evident that multipacting for the lower RF power ranges has been eliminated by the RF processing. For higher

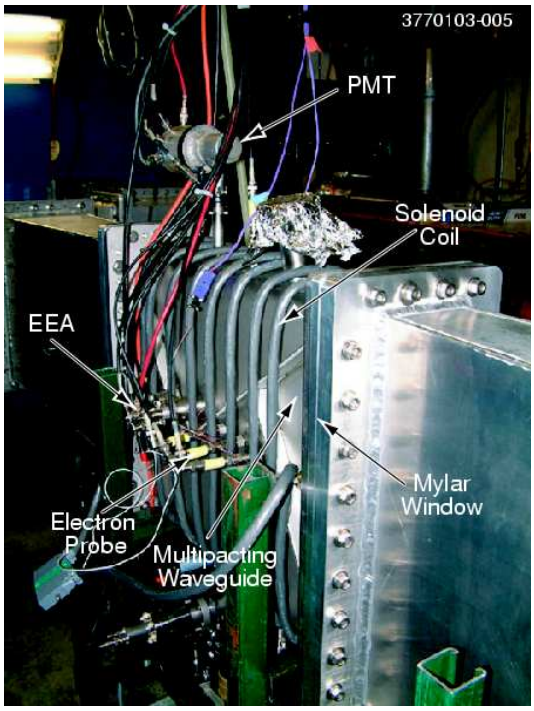

Fig. 5. Photo of the multipacting waveguide with the solenoid coil. Shown also are various diagnostic sensors.

power ranges, a stable multipacting current persists even after an extended processing period.

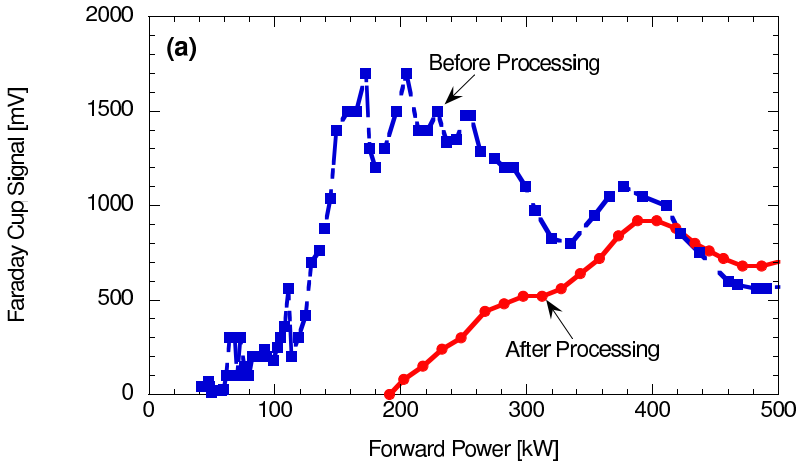

Fig. 6. Multipacting current before and after RF processing.

After RF processing, the multipacting current measurements were repeated at various power levels so that the complete multipacting band was mapped out for the power range of interest. Fig. 7 shows the multipacting current as measured by the electron pick-up probe P2 for different modes, including the traveling wave mode (TW), the standing wave mode (SW) and the mixed wave mode (MW) with a reflected power ratio of 16.6%.

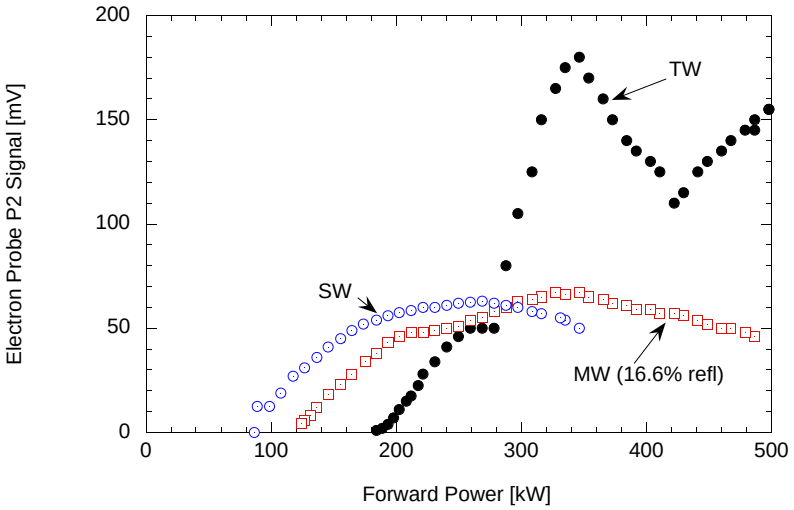

Fig. 7. Multipacting current for the traveling (TW) mode, standing wave (SW) mode and mixed wave (MW) mode with a 16.6% reflection ratio.

3.2 Suppressing multipacting with bias magnetic fields

By running a DC current through the solenoid coil, a DC magnetic field was generated in the waveguide space. The effect of this bias magnetic field is immediate. Without the solenoid field, the RF power was frequently cut off during the processing period due to PMT light trips which were always accompanied by an increase of the waveguide pressure. When a bias magnetic field was maintained at a proper level, the RF could stay steadily at the desired power level without any PMT light trip. In the mean time, the pressure in the waveguide remained very stable. However, When the solenoid field was removed by turning off the coil current, all the multipacting symptoms (PMT light tripping, waveguide pressure increasing) resumed immediately. These observations are illustrated in Fig. 8.

The effect of the bias magnetic field was studied quantitatively by scanning the coil current after the RF processing was completed and a stable multipacting current obtained. Fig. 9 depicts the typical bias magnetic field (Bz) dependence of the multipacting current detected by the Faraday cup of the EEA for forward powers of 250 kW and 297 kW in the traveling wave mode. The polarity of the bias magnetic field is determined by the direction of the DC current flowing in the solenoid coil. A positive Bz means a bias magnetic field in the wave propagation direction, and a negative Bz means the opposite. A -100 V voltage was applied to the retarding grid of the EEA during the measurement. As one can see, both field polarities have a similar effect in affecting the multipacting current. The slight asymmetry is probably due to the fact that the multipacting electrons drift along the wave propagation direction, as revealed by the code Xing [10]. From Fig. 9 it is seen that very effective multipacting suppression can be realized when the bias field ampli-

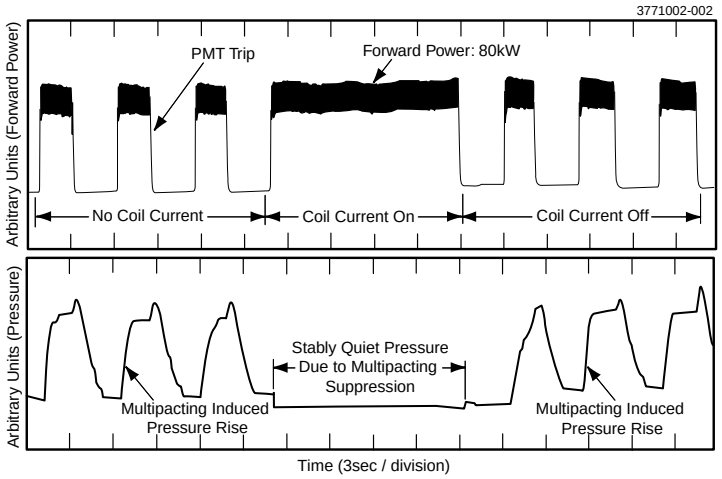

Fig. 8. Effect of the bias magnetic field generated by the solenoid coil. Without the bias field, PMT light trip frequently occur accompanied by a pressure rise in the waveguide; with the bias field, no PMT light trip is detected and the waveguide pressure remains quiet.

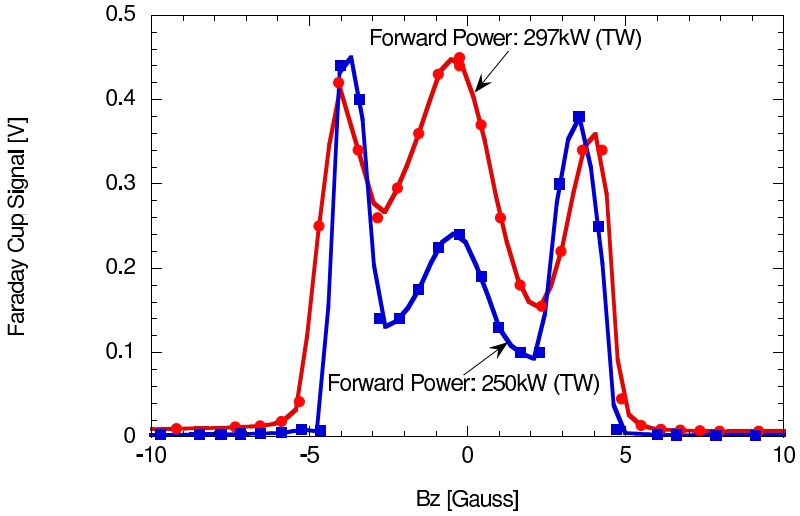

Fig. 9. Effect of a bias magnetic field on the multipacting current.

tude is above the level which we call the suppression bias field. For a forward power of 297 kW in the TW mode, the suppression bias field, denoted as B_s, is about 6 Gauss.

3.3 Anomalous multipacting enhancement

An unexpected effect observed during the tests with bias magnetic fields is that the multipacting current is enhanced at an intermediate bias field between 0 and B_s, as is evident in Fig. 9.

Without the bias magnetic field, multipacting electrons progressively develop in the central plane perpendicular to the broad walls of the waveguide. The multipacting electrons collide with the broad wall surface at normal incidence. When a longitudinal bias magnetic field exists in the waveguide space, the trajectories of multipacting electrons are bent away from the central plane. Multipacting electrons then collide with the broad walls at an inclined angle. Since the secondary electron emission coefficient has a strong dependence on the incident angle [15], the multipacting current is therefore enhanced. A higher bias field results in a higher degree of deviation from normal incidence, and hence a greater degree of multipacting enhancement. However, a high bias field will bend the trajectories to such a degree that the electrons will never collide with the broad walls. In this case, the multipacting will instead be suppressed.

3.4 Critical bias magnetic field

The bias field at which the electron trajectory is just crossing between the broad walls, and for which the enhancement is maximized by glancing incidence, is thereafter termed the critical bias magnetic field and denoted B_z^*. A simplified model has been developed to correlate B_z^* and the forward power in the TW mode. The underlying assumption of the theory is that the multipacting electron moves at a constant speed, which is the time average of its actual sinusoidal velocity. By equating the cyclotron radius of the hypothetical "steadily moving" electron with the narrow dimension of the waveguide, the following equation is derived for B_z^*,

$$B_z^* = \sqrt{\frac{4\mu_0 P_f}{k\omega a b^3}}, \tag{1}$$

where P_f is the forward power, k the wave propagation constant, μ_0 the permeability of vacuum, ω the angular RF frequency, and a and b the wide and narrow dimension of the waveguide respectively.

Inserting the parameters for the CESR type coupler waveguide, the critical bias field in practical units becomes

$$B_z^*[Gauss] = 0.21\sqrt{P_f[kW]}. \tag{2}$$

The results of this simple theory, as well as the experimental results measured from the Faraday cup current, are given in Fig.10. Also given in the figure are results of a numerical calculation, for which no "constant speed" assumption is made. The measured results are systematically higher than the theoretical

predictions. This may well be explained by the fact that the narrow dimension of the test waveguide is actually smaller than the 4″ design value, because of the wall deflection under the load of the atmosphere pressure. Another theoretical curve for a 3″ high waveguide (the same width) is given also in Fig.10. It can be seen that the experimental results fall reasonably within the constraints set by the theory.

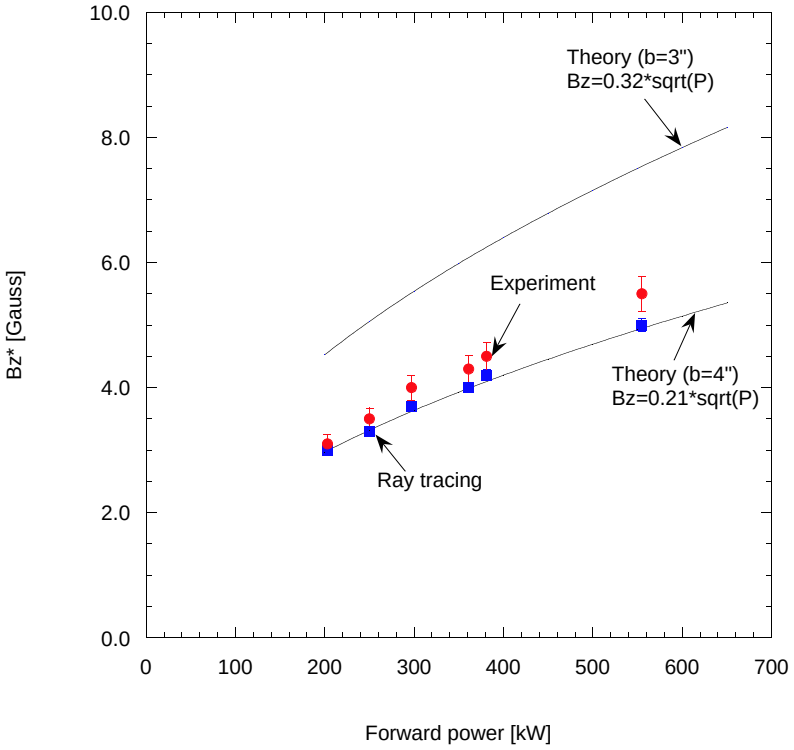

Fig. 10. Critical bias magnetic field for CESR type coupler waveguide. Red solid circle: experiment; Blue solid square: numerical calculation; Black solid lines: Theory for a 4″ and 3″ height respectively.

At a bias field higher than B_z^*, multipacting becomes quickly suppressed. A rigorous theoretical description of the suppression bias field is not pursued here. However, it is experimentally observed that above $2B_z^*$, complete multipacting suppression can be achieved. Ultimately, we have a very simple formula for the suppression bias magnetic field B_s

$$B_s = 4\sqrt{\frac{\mu_0 P_f}{k\omega a b^3}}. \tag{3}$$

Eq. 3 can be used to determine the bias magnetic field needed to fully suppress the multipacting in a rectangular waveguide of any size at any power level in the TW mode.

3.5 Bias field effect on multipacting in the SW mode

The bias magnetic field effect for the SW (full reflection) mode becomes more involved, as shown in Fig. 11. The P2 current is shown as a function of the bias field for forward powers of 146 kW and 203 kW. In contrast to the case for the TW mode, no complete multipacting suppression was achieved, at least within the field range that we could produce with our solenoid coil, which is between -20 and 20 Gauss. There seems to be a second multipacting enhancement peak after the first one near 4 Gauss. This effect is yet to be further explored to characterize its nature. From a practical point of view, one should not be too much concerned with this situation. The reason is that a coupler waveguide will be normally operating in the TW mode or MW mode (with only a small amount of reflection). However, this anomalous enhancement effect may be useful to promote processing in SW mode, which is needed sometimes before a module is installed in a machine.

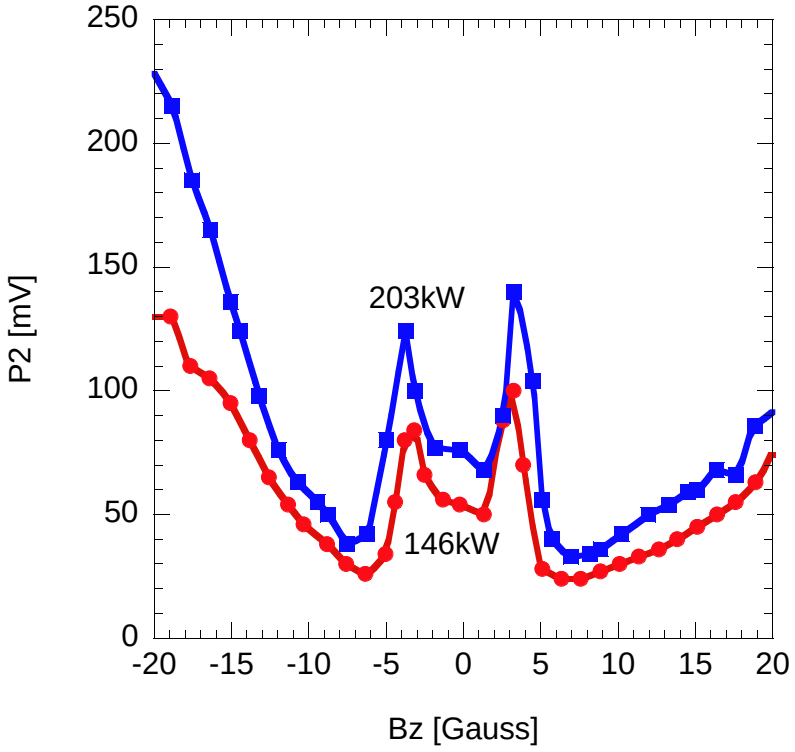

Fig. 11. Effect of a solenoid bias field on the multipacting in the waveguide in the SW mode.

4 Slotted waveguide

Simulations with the code Xing revealed that long lifetime resonant electron trajectories exist only in the central plane perpendicular the broad walls of

the waveguide. It has been predicted that multipacting can be effectively suppressed effectively by opening a longitudinal slot in the center of the broad walls [11]. One of the major goals of the present study has been to verify the concept of slotted waveguide.

The details of the slot are given in Fig.12. The slot is cut out on a copper bar that is bolted to a stainless steel insert, which in turn is fitted into a groove box welded onto the bottom wall of the waveguide. The insert flange is sealed against the groove box flange with a Viton O-ring. This design leaves a large degree of flexibility by replacing the copper bar with other ones with alternative slot shapes or simply with different materials or surface coatings. The first copper bar bears a 5 mm wide slot. The two side walls of the slot have different depths, 5 mm for one and 10 mm for the other. For this reason, the floor of the slot ends up with a 45° slope. The slope is expected to further promote multipacting suppression by redirecting the secondary electrons from the bottom to the 10 mm sidewall where they will be absorbed.

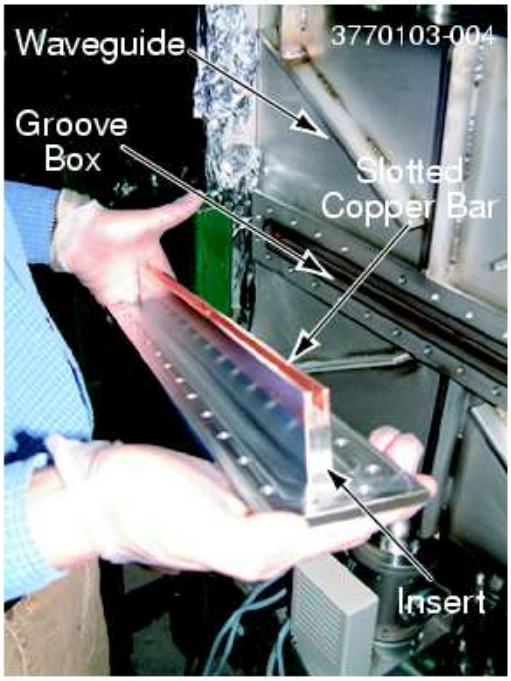

Fig. 12. Photo of the slotted waveguide.

4.1 Suppressing multipacting with a slot on the broad wall

Fig. 13 shows the effect of the slot. A factor of 2 to 7 reduction in the multipacting current as measured by the P2 probe was obtained. The power level at which multipacting first occurs is slightly increased, but it is obvious that complete multipacting suppression is not achieved with the slot.

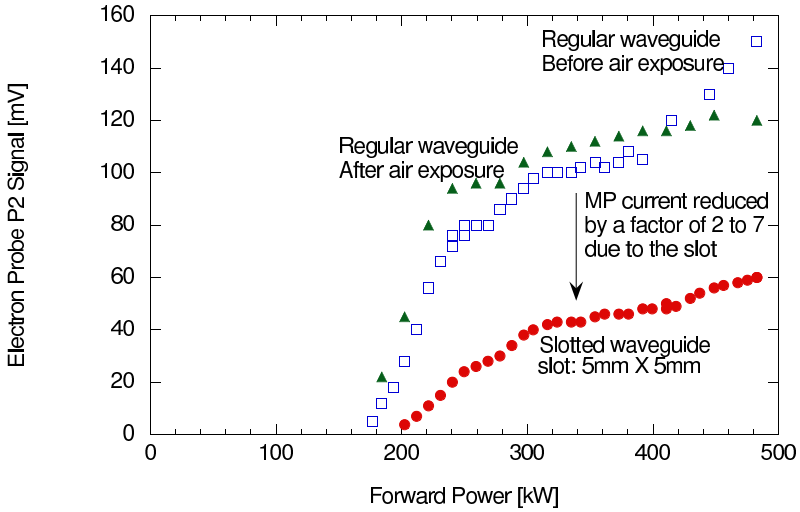

Fig. 13. Suppression of multipacting by a 5 mm wide slot opened along the high electric field region of the broad wall.

Besides reducing the multipacting current for a given power level, the slot has another beneficial effect. RF processing becomes much quicker above 180 kW, as indicated by a reduced number of PMT light trips whereas for a regular waveguide, quick processing comes much later, at 270 kW. This difference is shown in Fig.14.

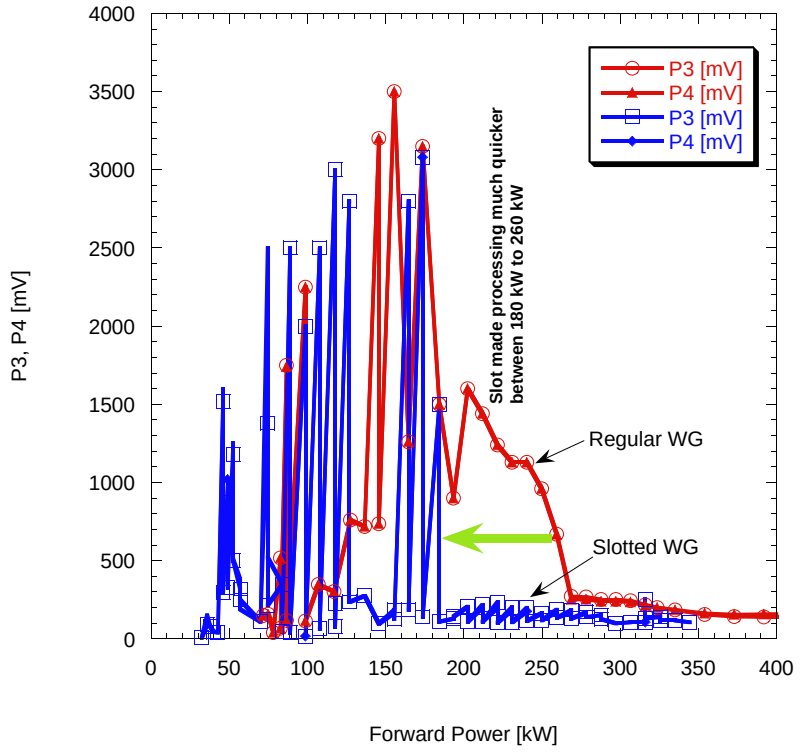

Fig. 14. Benefit of the slotted waveguide: quicker processing above 180 kW; while it comes only above 270 kW for regular waveguide.

4.2 Slot varieties

Test results with different copper bars are given in Fig. 15. With a flat copper bar (solid circle in Fig. 15) the slotted waveguide degenerates into a regular waveguide whose multipacting characteristics may be compared to those when the waveguide is fitted with various inserts, including the slotted copper bar described in Sec. 4.1 (Solid square), the same bar but freshly etched (empty circle), and with the bar removed (solid triangle). In the later case, a 12 mm wide by 15 mm deep square slot is resulted. As one can see, there is little difference due to the change in the feature of the inserts. The fact that reduction in multipacting current is rather insensitive to changes in slot dimensions suggests that multipacting develops not exclusively in the narrow volume in the center plane, but a significant contribution comes from electrons hitting the broad walls outside of this central volume. In our test, only the bottom wall was fitted with a slot. We believe a further improvement of multipacting suppression can be realized by opening a similar slot in the top wall of the waveguide. It should be pointed out that the dimensions of the slot have been kept small to get effective RF cut off and small impedance mismatch due to the presence of the slot.

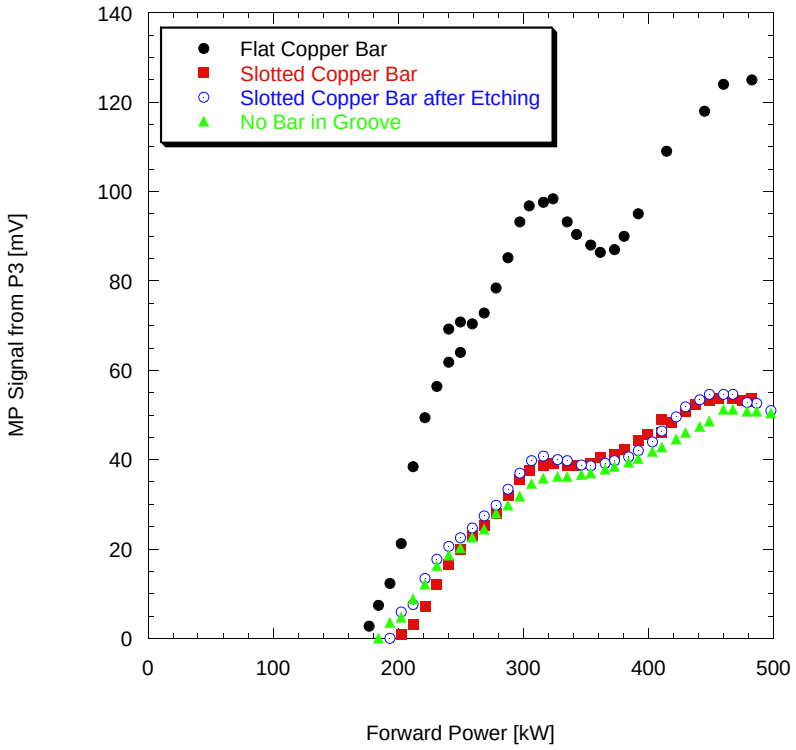

Fig. 15. Effect of different slots.

Finally, we would like to evaluate if the earth magnetic field has any effect on the slot waveguide experiments. To the first order, we are only concerned with the field component in parallel to the broad walls of the waveguide, which

was measured to have a maximum value of 0.24 Gauss is the test area. The cyclotron radius of the secondary electrons in the slot space in the presence of this field is calculated to be on the order of 200 mm. This is to be compared to a 10 mm characteristic dimension of the slot. We then conclude that the earth magnetic field has played a negligible role in the slot waveguide experiments.

5 Conclusion

Multipacting in the CESR type rectangular waveguides was experimentally confirmed to exist. Multipacting starts at a power level as low as 40 kW for a fresh waveguide surface. Multipacting barriers below 180 kW are "soft" and can be eliminated by RF processing. Above 180 kW, multipacting becomes so "hard" that it persists even after an extended RF processing period. The hardness of multipacting barriers is explained by the difference in the impact energy of multipacting electrons. Xing calculations and measurements with the EEA both revealed that the impact energy of multipacting electrons is linearly dependent on the RF power. It has been shown that for a lower impact energy, the secondary emission coefficient can be dramatically reduced when a surface has been "cleaned up" by RF processing [15]. For a higher impact energy, as for multipacting at higher RF power ranges, the secondary emission coefficient is rather insensitive to RF processing.

To suppress the "harder" multipacting barriers at higher RF power levels, the slotted waveguide method has been shown to be beneficial. The multipacting current is cut down by a factor of 2 to 7 with one slot on the bottom wall. The RF processing of the slotted waveguide is much quicker above 180 kW. A further multipacting suppression can be expected with a pairing slot on the top wall. Experimentally, the multipacting induced discharge is found to exist over a broad region across the broad dimension, despite the prediction of simulations that multipacting develops only in a narrow zone around the central plane. One may have to open multiple slots on broad walls to achieve complete suppression with the slotted waveguide method.

Complete multipacting suppression can be realized by using the bias magnetic method. A general formula has been derived to determine the bias magnetic field needed for full multipacting suppression in a rectangular waveguide of any size at any power level. For the CESR type waveguide geometry, a mild 10 Gauss bias field is sufficient to suppress multipacting below 550 kW. New cryo-modules for the CESR upgrade have all been equipped with solenoid coils for multipacting suppression.

When applying the magnetic bias method to a coupler of a superconducting RF cavity, it is advisable to keep the biasing field off when the cavity is passing

through superconducting transition during the cooling down period. Otherwise, the flux of the fringing bias magnetic fields, if they reach the vicinity of the cavity, will be trapped in the cavity material and result in a lower cavity quality factor. However, one should not be concerned with the fringing field when the cavity is already superconducting. The reason is that the needed bias magnetic field (on the order of 10 Oe) is trivial compared to the lower critical field H_{c1} of niobium. The cavity will be still in the Meissner state even in the presence of this fringing field. For these reasons, the biasing field is not expected to affect the cavity in an undesirable way. One of the CESR cryo-modules has been in operation over long term with an activated elbow coil. No adverse effect on the superconducting cavity performance has been observed due to the bias magnetic field.

We should point out that a similar suppression effect can be anticipated for the multipacting in coaxial waveguide couplers because the trajectory of multipacting electrons is expected to bend in a similar fashion. The advantage of the magnetic bias method when applied to a coaxial coupler as compared to the electric bias method is that no insulation is needed between the inner and outer conductors. As an insulator will deteriorate over time, the magnetic bias method is therefore expected to provide better machine reliability in the long term.

6 Acknowledgment

This work is supported by the National Science Foundation. We thank John Reilly, Phil Barnes and James Sears for their help with many aspects of the test.

References

[1] J. Tückmantel et al., Improvements to power couplers for the LEP2 superconducting cavities, Proceedings of the 1995 Particle Accelerator Conference and International Conference on High-Energy Accelerators, Dallas, Texas, USA, (1996)p1642.

[2] E. Somersalo, Y. Ylä-oijala, D. Proch, Analysis of multipacting in coaxial lines, Proceedings of the 1995 Particle Accelerator Conference and International Conference on High-Energy Accelerators, Dallas, Texas, USA, (1996)p1500.

[3] P. Ylä-Oijala, Analysis of electron multipacting in coaxial lines with traveling and mixed waves, TESLA report, TESLA 97-20.

[4] G. Devanz, A 2D multipacting simulation code for RF components and accelerating cavities, Proceedings of the 2000 European Particle Accelerator Conference, Vienna, Austria, (2000)p1366.

[5] P. Ylä-Oijala, Suppressing electron multipacting in coaxial lines by DC voltage, TESLA report, TESLA 97-21.

[6] Y. Kijima et al., Input coupler of superconducting cavity for KEKB, Proceedings of the 2000 European Particle Accelerator Conference, Vienna, Austria, (2000)p2040.

[7] M. Stirbet et al., High power RF tests on fundamental power couplers for the SNS project, Proceedings of the 2002 European Particle Accelerator Conference, Paris, France, (2002)p2283.

[8] M. Stirbet, private communications.

[9] S. Belomestnykh et al., Commissioning of the superconducting RF cavities for the CESR luminosity upgrade, Proceedings of the 1999 Particle Accelerator Conference, New York City, USA, (1999)p980.

[10] R.L. Geng and H. Padamsee, Exploring Multipacting Characteristics of a Rectangular Waveguide, Proceedings of the 1999 Particle Accelerator Conference, New York City, USA, (1999)p429.

[11] R.L. Geng, H. Padamsee, V. Shemelin, Multipacting in a Rectangular Waveguide, Proceedings of the 2001 Particle Accelerator Conference, Chicago, USA, (2001)p1228.

[12] R.L. Geng and H. Padamsee, Condensation/Adsorption and Evacuation of Residual Gases in the SRF System for the CESR Luminosity Upgrade, Proceedings of the 1999 Particle Accelerator Conference, New York City, USA, (1999)p983.

[13] R.A. Rosenberg, K.C. Harkay, Nuclear Instruments and Methods in Physics Research A 453(2000)507-513.

[14] H. Seiler, J. Appl. Phys. 54(1983)R1; H. Bruining, Physics and Application of Secondary Electron Emission, Pergamon Press, Oxford, 1954.

[15] V. Baglin et al., The secondary electron yield of technical material and its variation with surface treatments, Proceedings of the 2000 European Particle Accelerator Conference, Vienna, Austria, (2000)p217.